ACS OMEGA

Open Access



http://pubs.acs.org/journal/acsodf

Article

# Preparation of Open-Cell Long-Chain Branched Polypropylene Foams for Oil Absorption

Chenhui Li, Jirun Hu, Haikuo Yan, Yuyuan Yao, Li Zhang,* and Jinbiao Bao*

Cite This: *ACS Omega* 2023, 8, 49372−49382

Read Online

ACCESS | Metrics & More | Article Recommendations | Supporting Information

**ABSTRACT:** This study aimed to prepare open-cell foams using a blend of long-chain branched polypropylene and polyolefin elastomer (LCBPP/POE) for the production of reusable oil absorbents. The supercritical $CO_2$ foaming process was conducted using a two-step batch rapid depressurization method. This unique two-step foaming approach significantly expanded the temperature and pressure windows, resulting in more uniform cells with smaller sizes, ultimately leading to higher expansion ratios and an increased open cell content. The foaming process was optimized by adjusting parameters, such as the LCBPP/POE ratio, foaming temperature, and foaming pressure, reaching a maximum open cell content of 97.6% and a maximum expansion ratio of 48. The influence of polypropylene (PP) crystallization was investigated with the aid of scanning electron microscopy and differential scanning calorimetry. Furthermore, the hydrophobic and lipophilic characteristics of the LCBPP/POE open-cell foam were determined *via* contact angle measurements and oil/water separation tests. Oil absorption tests revealed that the blended LCBPP/POE foam has a higher oil absorption capacity than that of the pure LCBPP foam. The cyclic oil absorption tests demonstrated the outstanding ductility and recoverability of the LCBPP/POE open-cell foam in comparison to those of the pure LCBPP foam. Over 10 cycles, the LCBPP/POE foam maintained a substantial adsorption capacity, retaining 99.3% of its initial oil absorption capacity. With its notable features, including a high open cell content, excellent hydrophobic and lipophilic characteristics, superior oil absorption capacity, impressive cyclic oil absorption performance, and robust reusability, LCBPP/POE open-cell foams exhibit significant promise as potential oil adsorbents for use in oil spill cleanup applications.

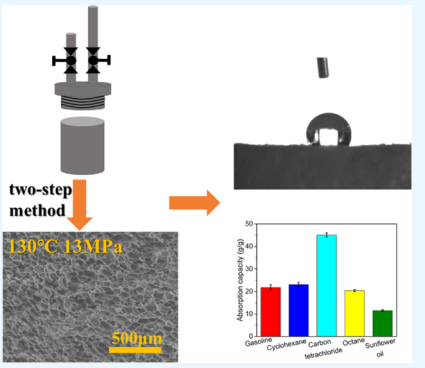


## 1. INTRODUCTION

In recent years, oil spills have continued to pose environmental challenges, resulting in severe ecological and environmental pollution due to near-shore petroleum leaks and industrial waste oil emissions. As a result, addressing oil spill cleanup has become an urgent priority for global environmental protection and sustainable development.[1−4] Various cleanup methods have been explored, including on-site incineration, oil containment booms, bioremediation, dispersants, and oil absorbents.[5−8] Among them, oil absorbents have proven to be effective and cost-efficient solutions to this issue.

Recent reports have highlighted open-cell polymer foams as the preferred choice for oil absorbents, such as polyurethane sponges,[9−11] polylactic acid foams,[12,13] and polyolefin foams.[14−20] For instance, Wu et al. successfully prepared superhydrophobic polyurethane sponges that exhibited a petrol absorbency of 13.26 g/g.[10] Similarly, Wang et al. prepared open-cell polylactic acid foam with an oil absorbency of 5 g/g.[12] However, these sponges exhibit some degree of hydrophilicity and require additional modifications to enhance their hydrophobic properties, significantly increasing their cost.

From the perspective of lipophilicity, polyolefin open-cell foams are preferred and have gained considerable attention. Sun et al. conducted research on modifying high-density polyethylene aerogels with reduced graphene oxide, achieving a gasoline absorption of 7.8 g/g.[21] However, the inherent poor compression resilience of the polyethylene foam still necessitates improvements in its repetitive oil absorption capacity.[22,23] In our previous studies, we explored open-cell foams comprising polypropylene (PP)/ethylene propylene diene monomer (EPDM) for oil absorption applications.[24,25] Regrettably, the low expansion ratio (ER) posed a significant limitation on the oil absorption capacity. Mi et al. utilized twin-screw extrusion and supercritical carbon dioxide foaming to fabricate PP/poly(tetrafluoroethylene) (PTFE) composite foams by blending nanosized PTFE particles with PP, yielding commendable oil absorption performance.[20] Zhao et al. developed a superhydrophobic PP/CNT/sorbitol derivative nanocomposite open-cell foam by polymer blending and the subsequent foaming process, demonstrating excellent oil absorption efficiency and high reusability.[26] Nonetheless, the high cost associated with PTFE particles and carbon nanotubes

Received: October 10, 2023
Revised: November 30, 2023
Accepted: December 4, 2023
Published: December 14, 2023

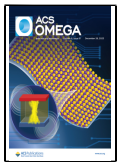

renders them unsuitable for widespread industrial application. Pang et al. conducted a study where they blended PP with a polyolefin elastomer (POE) to manufacture open-cell foams through continuous extrusion foaming, enhancing the foam's oil absorption capacity and resilience.[27,28] While these methods have exhibited promising outcomes, there is still significant room for improvement, particularly in achieving foams with an expansion ratio (ER) exceeding 40 and an open cell content exceeding 95%.

Many previous studies have primarily focused on the utilization of conventional linear polypropylene materials.[29−34] However, linear polypropylene exhibits a limited foaming range and faces challenges in achieving high-ER foams due to its melt strength being highly sensitive to temperature fluctuations. Moreover, linear polypropylene tends to generate open-cell structures with larger cell sizes (>250 $\mu$m), which are less conducive to effective oil−water selectivity.

To enhance the ER and regulate the cell size, long-chain branched polypropylene (LCBPP) emerges as a promising alternative.[35−40] Nonetheless, generating foams with a high degree of open-cell structure from LCBPP presents its own set of challenges, and there is a scarcity of literature detailing the utilization of LCBPP in open-cell structure preparations.

In this study, polyolefin elastomers (POE) were introduced to LCBPP to promote cell opening and enhance compression resilience. The supercritical $CO_2$ foaming of the LCBPP/POE blend was conducted using a two-step batch rapid depressurization method. The study delved into the impact of saturation temperature and pressure on the cell morphology, ER, and open cell content (OCC). Moreover, simulation experiments were carefully carried out to examine the LCBPP crystallization behavior during the saturation process, assess the influence of LCBPP's crystalline structure on foam morphologies, and explore the possible cell-opening mechanism. Moreover, the oil sorption capacity was validated, and the reusability of the open-cell LCBPP/POE foam was investigated through cyclic adsorption−desorption experiments.

## 2. EXPERIMENTAL SECTION

**2.1. Materials.** The LCBPP was supplied by Zhenhai Refining and Chemical Company, with a melting temperature of 154 °C and a melt flow index of 1.7 g/10 min (measured at 230 °C and 2.16 kg), and the melt strength of LCBPP material is 0.174 N at 180 °C measured using a RHEOTENS 71.97 (Göttfert Ltd., Buchen, Germany); the details of the experiment are shown in the Supporting Information (SI). Dow Chemical provided the POE (EG8100) with a melt flow index of 1 g/10 min. $CO_2$ (purity: 99%) was supplied by Ningbo Fangxin Gas Co., Ltd. Xylene was obtained from the China National Pharmaceutical Group Corporation. Gasoline, cyclohexane, carbon tetrachloride, and octane were used in the oil absorption experiment.

**2.2. Preparation of LCBPP/POE Blends.** The LCBPP pellets were placed in an oven and dried at 60 °C for 4 h prior to extrusion to remove moisture. A series of LCBPP/POE blends in the ratios of 100, 90/10, 80/20, 70/30, and 60/40 were prepared using a HAAKE Mini Lab twin-screw extruder (Thermo Electron, Germany) at 180 °C for 3 min at 30 rpm, which were named PP, PP9/POE1, PP8/POE2, PP7/POE3, and PP6/POE4, respectively. The obtained melt was extruded directly into a heated cylinder and injected into a 2 mm-thick die using a Haake MiniJet (Thermo Electron, Germany).

**2.3. Preparation of the Polymer Foam.** The foaming process was carried out in a molding machine. For the one-step foaming process, the 2 mm-thick flakes were placed in the mold cavity after the temperature is raised to the specified temperature and saturated with $CO_2$ for 2 h, and then, the mold was quickly opened to obtain foams. For the two-step foaming process, the flakes were placed into an autoclave, which can withstand high pressures (up to 30 MPa). First, the flakes were saturated at 180 °C for 20 min to melt the crystalline region. Subsequently, the samples were cooled to the foaming temperature in the range of 120−137 °C and the saturation pressure range was from 10 to 20 MPa and held for 30 min before the $CO_2$ was released by rapidly opening the valve. Once the $CO_2$ is fully released, the vessel is quickly opened, and the foam sample is removed for subsequent analysis. Each foaming process is performed in the vessel after $CO_2$ is released.

**2.4. Treatment of Annealed Samples.** This step is basically the same as the preparation of the polymer foam mentioned above; the difference is that after lowering the temperature to the foaming temperature range and saturating for 30 min, the valve is opened slowly to avoid foaming of the sample. After waiting for the complete release of $CO_2$, the vessel is cooled to ambient temperature in a water bath, and the annealed sample was removed, which was immersed in liquid nitrogen for 3−5 min and then broken. The samples were heated in xylene to 60 °C and soaked for 4 h to remove the POE from the annealed samples. The samples were sprayed with Pt in a vacuum chamber and then photographed by scanning electron microscopy (SEM, TM3000).

**2.5. SEM Measurement.** The morphology of the LCBPP/POE foam was photographed with a (TM3000, Hitachi, Japan) scanning electron microscope. The samples were immersed in liquid nitrogen for 3−5 min and then fractured. The cross-section of the sample was photographed by scanning electron microscopy after Pt was sprayed in a vacuum chamber.

**2.6. Differential Scanning Calorimetry (DSC) Measurements.** Differential scanning calorimetry (DSC-25, TA) was used to study the nonisothermal crystallization behavior of LCBPP and LCBPP/POE blends. The sample mass was about 10 mg, the purge atmosphere was $N_2$, and the temperature was increased from 40 to 200 °C at 10 °C/min and kept constant for 10 min. After eliminating the thermal history, the temperature was decreased from 200 to 40 °C at a cooling rate of 10 °C/min.

**2.7. Measurement of Sample Properties.** The mass density of the samples before foaming ($\rho_v$) and after foaming ($\rho_f$) was measured by the water displacement method according to ISO 1183-1987. $\varphi$ is the expansion ratio of the foam and can be calculated by the formula

$$\varphi = \frac{\rho_v}{\rho_f}$$

At least three tests were performed for samples prepared under the same conditions, and the average value was calculated. The open cell content of the LCBPP/POE foam was estimated using an accurate density meter (UltraFoam 1000) according to the ISO 4590 standard. Five measurements were made for each sample, until the error was less than 0.005%. The value of the open cell content is the average of three pieces. The open cell content (OCC) of the foam was


https://doi.org/10.1021/acsomega.3c07915
ACS Omega 2023, 8, 49372−49382

measured using a gas displacement density analyzer (AccuPyc II 1340, Micromeritics) according to the following equation

$$\mathrm{OCC} = \frac{V_{\mathrm{open}}}{V_{\mathrm{total}}} = 1 - \frac{V_{\mathrm{ture}}}{V_{\mathrm{total}}}$$

where $V_{\mathrm{open}}$, $V_{\mathrm{true}}$, and $V_{\mathrm{total}}$ are the open cell volume, true volume (including closed cell volume and cell wall volume), and total volume of the foam, respectively.

**2.8. Oil Absorption Test.** The oil and cyclic oil absorption tests were conducted at room temperature. The open-cell foam was first weighed and then externally immersed in a 100 mL beaker. After saturation, the foam was removed from the oil and quickly weighed. The oil absorption capacity of the open-cell foam was derived from the following equation

$$\text{oil sorption (g/g)} = \frac{m_s - m_0}{m_0}$$

where $m_0$ is the dry open-cell foam sample's weight and $m_s$ is the open-cell foam sample's weight after saturating with the adsorbed target oil. For the cyclic oil adsorption experiment, the open-cell foam was cut into rectangles with a length of about 2 cm and then weighed as $m_0$. After that, the foam was immersed in oil adsorbed until reaching a saturation weight, $m_1$. The adsorption capacity $[(m_1 - m_0)/m_0]$ was obtained for the first adsorption. Subsequently, the oil in the foam was squeezed out as much as possible, and then, the foam was weighed as $m_{10}$ to obtain the recovery capacity $[(m_{10} - m_0)/m_0]$ for the first desorption. Subsequent cycles (2nd−10th) of adsorption and desorption were performed similarly to obtain the corresponding adsorption and recovery capacities.[41−44]

## 3. RESULTS AND DISCUSSION

**3.1. Exploration of the Foaming Strategy.** Initially, a one-step LCBPP/POE foaming process was carried out in the temperature range of 150−156 °C at a pressure of 15 MPa. As shown in Figure 1, the PP7/POE3 foams exhibited a hexagonal cell shape when foamed using the one-step method, achieving an expansion ratio (ER) of approximately 20, and the cell size of the foam gradually decreases as the temperature increases, from 74 μm at 150 °C to 58 μm at 156 °C. However, the foams predominantly presented a closed-cell structure and cannot be foamed below 150 °C or above 156 °C. Below 150 °C, the increased melt strength hinders the foaming process, resulting in an ER of less than 3. If the foaming temperature is above 156 °C, then, the low melt strength of the polymer melt causes the foam to lose its shape and collapse rapidly, leading to an unstable cell structure. As a result, it becomes evident that the one-step foaming method has a limited foaming range and is challenging to effectively control. As an oil-absorbing material, achieving a high open cell content (OCC) is imperative. However, the level of the OCC achieved through the one-step method typically does not exceed 60%. In the one-step foaming process, only the POE component of the LCBPP/POE blends contributes to the formation of an open-cell structure, resulting in a low open cell content. This limitation adversely affects the oil absorbing performance of the material.

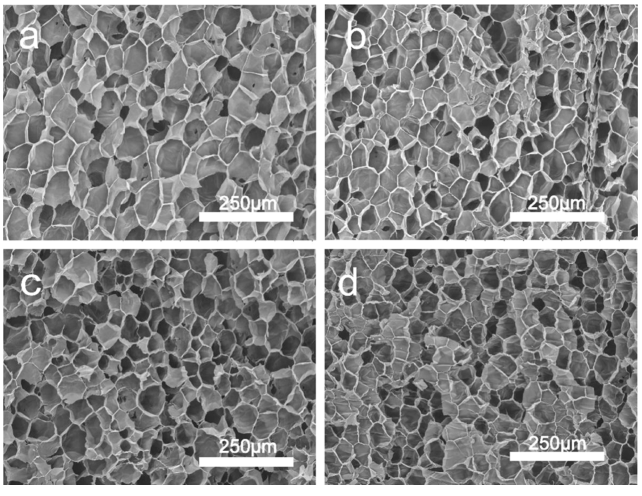


**Figure 1.** SEM micrographs of the foam samples under a one-step foaming method with a foaming pressure of 15 MPa and foaming temperatures of (a) 150 °C, (b) 152 °C, (c) 154 °C, and (d) 156 °C.

To further improve the ER and the OCC of the LCBPP/POE foam, a two-step foaming process was developed in this work. The LCBPP/POE samples were first saturated at 180 °C in $scCO_2$ conditions to completely melt the crystalline regions. Subsequently, the samples were cooled to the foaming temperature of 120−137 °C to improve the melt strength. Finally, the valve was open to release the compressed $CO_2$ rapidly to initiate the foaming process.

Figure 2 displays the SEM micrographs of foam samples prepared using the two-step method with varying LCBPP/POE ratios at a temperature of 130 °C and pressure of 20 MPa. It reveals that the addition of the POE leads to an irregular cell morphology and a significant reduction in average cell diameter; the cell diameter of the PP7/POE3 foam reduces to 48 μm. The OCC measurements indicate a progressive increase in the values as the POE content gradually rises. The pure PP foam exhibits an OCC of 83.3%, while the PP9/POE1 foam has an OCC of 87.4%, the PP8/POE2 foam has an OCC of 93.8%, the PP7/POE3 foam has an OCC of 97.6%, and the PP6/POE4 foam has an OCC of 98.3%. Despite the exceptionally high OCC of the PP6/POE4 foam, the excessive addition of the POE resulted in the prepared foams being too fragmented to undergo cyclic oil absorption experiments. Consequently, the PP7/POE3 foam was selected as a case example, and its foaming parameters were examined. The impact of POE addition on the oil absorption and reusability performance of the LCBPP/POE foam was studied by comparing it with other foams containing different amounts of the POE.

**3.2. Influence of the Temperature and Pressure on the ER and OCC of the PP7/POE3 Foam.** It is widely acknowledged that the ER and the OCC of the foam are influenced by the foaming temperature and saturation pressure. Therefore, it is necessary to investigate their impact on the LCBPP/POE blends.

Figure 3a−g displays the SEM micrograph of the PP7/POE3 blend foaming at varying temperatures under a pressure of 15 MPa. The two-step foaming process exhibited a temperature range between 120 and 137 °C, showcasing a significant expansion compared to the one-step method. In Figure 3h, it can be observed that the ER initially rises and then declines as the temperature increases, peaking at 130 °C. Beyond 133 °C, a phenomenon of cell collapse becomes apparent, leading to a significant drop in the ER. Similarly, at 120 °C, the ER experiences a substantial decrease, plummeting to just 20. This behavior can be attributed to the fact that at 133 °C, the melt


https://doi.org/10.1021/acsomega.3c07915
ACS Omega 2023, 8, 49372−49382

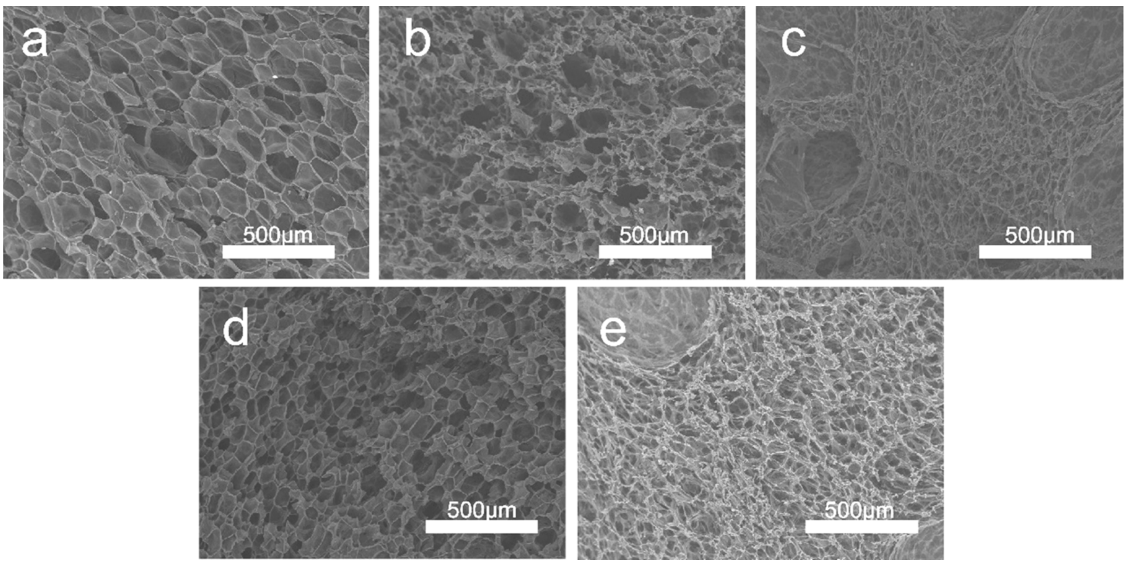


**Figure 2.** SEM micrographs of the foam samples under the two-step foaming method of (a) pure PP, (b) PP9/POE1, (c) PP8/POE2, (d) PP7/POE3, and (e) PP6/POE4 with a foaming temperature of 130 °C and a foaming pressure of 10 MPa.

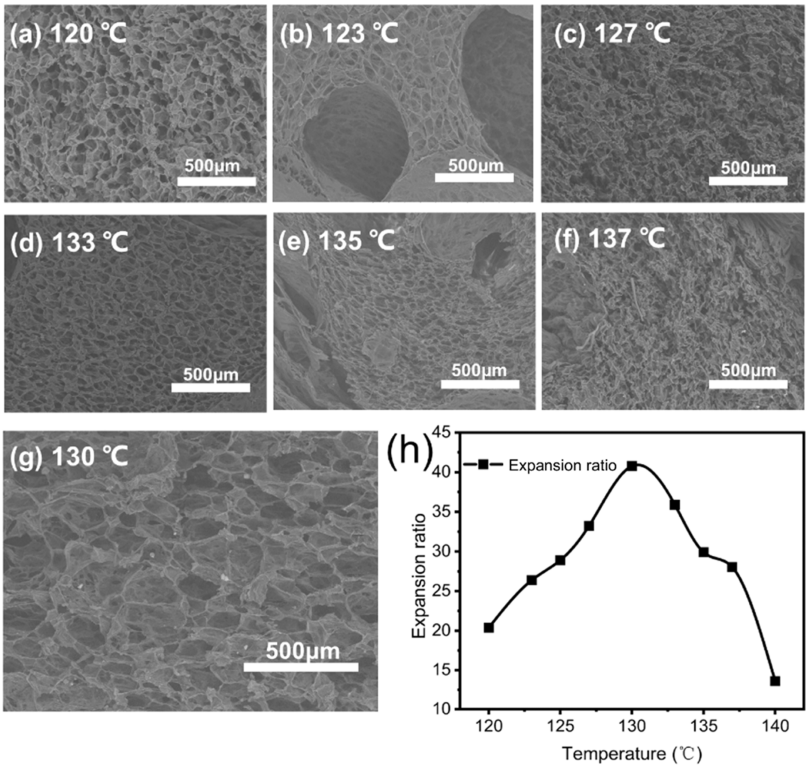


**Figure 3.** (a−g) SEM micrographs of PP7/POE3 foam samples at 15 MPa with different temperatures and (h) expansion ratio of the PP7/POE3 foam at different temperatures of 15 MPa.

strength is already considerably low, making it unable to adequately support the cell structure, resulting in partial cracking. In the case of 120 °C, excessive melt strength leads to a pronounced reduction in both the ER and the resulting OCC. Hence, 130 °C emerges as the optimal foaming temperature, where the ER reaches 40.8, and the resulting OCC surpasses 95%. In the process of exploring the relationship between the ER of the PP7/POE3 foam and temperature, it is noteworthy that the foam foaming at 123 °C exhibited a peculiar phenomenon of having large cell holes, some even reaching millimeter in diameter, as shown in Figure S1 in the SI. Subsequent oil absorption capacity testing revealed that the foam with these substantial cell holes displayed poor oil−water selectivity, absorbing both water and oil. When the water contact angle was measured, it became evident that water droplets penetrated the foam through these large cell holes. This situation hindered the desired oil−water separation performance, making it essential to analyze the underlying mechanism and explore methods to minimize this phenomenon, which will be discussed in detail later.

Figure 4 displays the SEM micrographs of the PP7/POE3 foams prepared at various saturation pressures. At a temper-



https://doi.org/10.1021/acsomega.3c07915
ACS Omega 2023, 8, 49372−49382

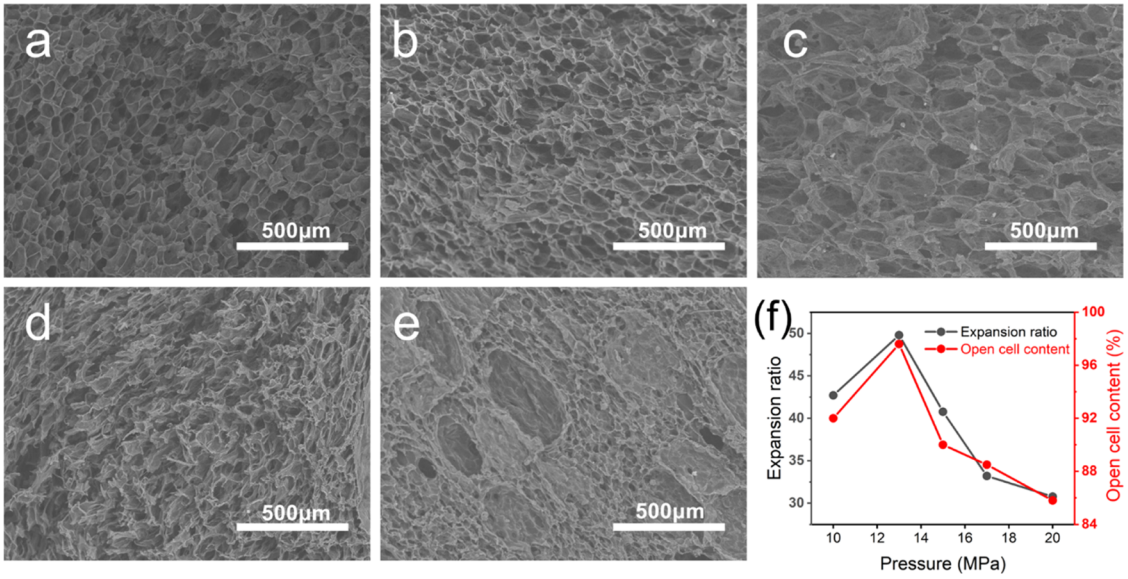


**Figure 4.** SEM micrographs of PP7/POE3 foam samples at 130 °C and (a) 10 MPa, (b) 13 MPa, (c) 15 MPa, (d) 17 MPa, and (e) 20 MPa and (f) diagram of the variation of the expansion ratio and open cell content of the PP7/POE3 foaming sample at 130 °C.

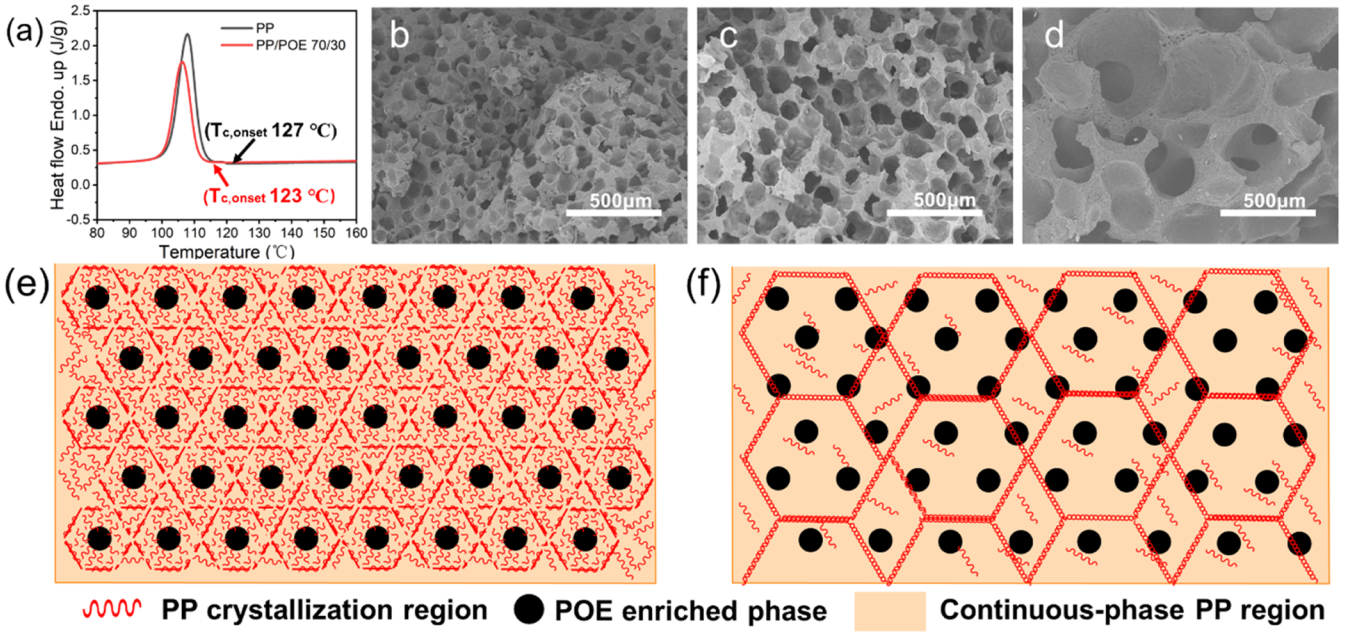


**Figure 5.** (a) DSC thermal analysis of the PP and PP7/POE3 blend; SEM micrographs of annealing treatments at (b) 120 °C, (c) 130 °C, and (d) 137 °C; and modeling of the crystalline structure of PP7/POE3 blends: at 120 °C (e) and at 137 °C (f); the small black dot represents the POE-enriched phase, the red wavy line represents the PP crystalline structure, and the orange part represents the continuous-phase PP region.

ature of 130 °C, the ER shows an initial increase followed by a decrease as the pressure increases. At 13 MPa, the ER reaches a maximum of 48 and the OCC can reach 97.6%. This phenomenon can be attributed to the fact that increased pressure promotes cell nucleation and enhances the availability of $CO_2$ for cell growth, thereby raising the foam's ER. As the pressure continues to increase, $CO_2$ solubility further increases and nucleation increases after rapid depressurization. However, excessive pressure reduces the melt strength, enabling $CO_2$ to escape from the matrix, which hinders cell growth and, consequently, leads to a gradual decline in the ER. The formation of an optimum open-cell structure requires a delicate balance of melt strength and cell growth. Open-cell structures generally require relatively low melt strength to rupture the cell walls. However, for the case at 17 and 20 MPa, excessively low melt strength can lead to excessive cell wall rupture, triggering severe cell coalescence and ultimately resulting in the vanishing of the open-cell structure.

### 3.3. Crystallization Behavior of the PP7/POE3 Foam.

The crystallization behavior during the foaming process has a direct impact on the ER and the OCC of the foam. DSC was utilized to investigate the crystallization of PP and PP7/POE3. The results are presented in Figure 5a. The crystallization temperature ($T_c$) of PP was 109 °C, the onset crystallization temperature ($T_{c,onset}$) of PP was 127 °C, and the exothermic crystallization enthalpy was 82.9 J/g. For PP7/POE3, $T_c$ decreased to 106 °C, $T_{c,onset}$ was 123 °C, and the exothermic crystallization enthalpy was 60.7 J/g. The decrease of $T_c$,


https://doi.org/10.1021/acsomega.3c07915
ACS Omega 2023, 8, 49372−49382

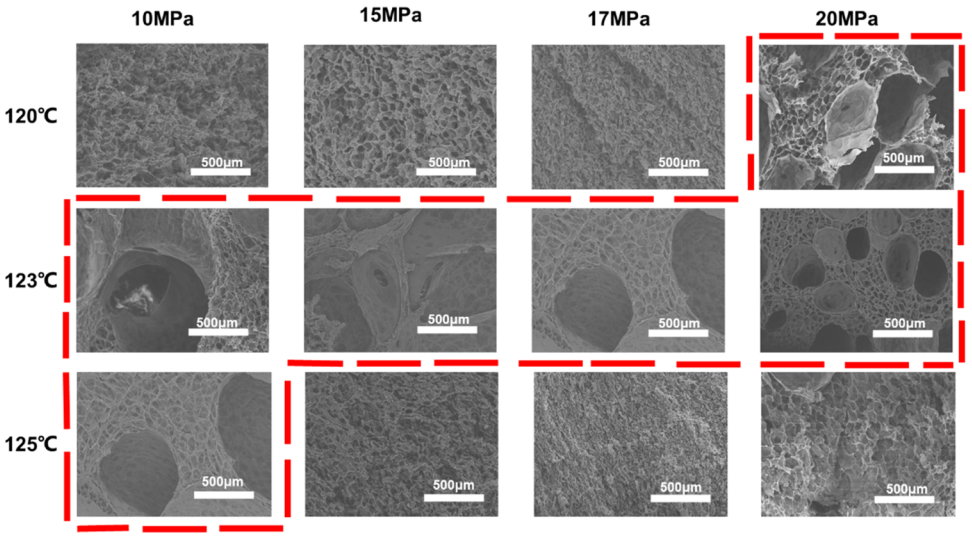


**Figure 6.** SEM micrographs of foamed samples at 120−125 °C. The red dashed box represents the appearance of large cell holes in the foam.

$T_{c,onset}$, and exothermic crystallization enthalpy was mainly due to the good compatibility between PP and the POE. At high temperatures, the flexible molecular chain of the POE interferes with the crystallization of the PP molecular chain, requiring lower temperatures for crystallization to occur. Consequently, it should be noted that in the PP7/POE3 foam prepared at temperature above 123 °C, the PP crystallization primarily occurred during the last step of pressure relief and cooling, rather than during the saturation process. In order to understand the crystallization of the PP7/POE3 foam, a simulation experiment was conducted. Initially, the samples underwent simulated two-step saturation treatment, which replicated the two-step foaming process, except for the final step of pressure relief foaming. In the two-step foaming process, the pressure was quickly released at the secondary step. However, in the simulation experiment, efforts were made to minimize foaming by slowly releasing the pressure, allowing for observation of the crystallization of PP in the sheet sample. Subsequently, the samples were embrittled using liquid nitrogen and etched with xylene. Our experiments demonstrated that xylene can not only etch away the POE region but also partially etch the PP amorphous region (for supporting evidence, refer to SI Figure S2: after pure PP was quenched by carbon dioxide at different temperatures, the etched PP amorphous region by xylene can be obviously observed in the SEM image). The etched cross-sections are depicted in Figure 5b−d.

At 137 °C, the cavitation in the etched part can reach a size of 200−300 $\mu$m in diameter. When the temperature is lowered to 120 °C, the size of the cavitation is reduced to 50 $\mu$m. It is important to note that all processing conditions remain unchanged during the two-step saturation treatment, except for the variation in the saturation temperature.

Considering that both PP and the POE chosen for this study have a melt flow rate below 2 g/10 min and the entire foaming process does not involve any mechanical mixing, it is difficult for the molecular chains of either PP or the POE to undergo molecular chain migration in the temperature range of 120−137 °C. This is primarily due to the high viscosity and lack of mechanical agitation. Therefore, the distribution of the POE in the PP matrix should be similar. (The pertinent evidence is presented in Figure S3.) If the crystallization states of PP in the samples were essentially the same, the SEM morphology after etching should also be similar. Therefore, the unusual appearance after etching is attributed to the significant change in the crystalline state of the PP following treatment at different saturation temperatures.

At the saturation temperature of 137 °C, which is significantly higher than the $T_{c,onset}$ of 123 °C for the PP7/POE3 blend, only minimal PP crystal nuclei may form during the saturation process. The primary crystallization occurred during the final stage of pressure relief and cooling, but it failed to create a grid-like crystallization network within the PP matrix. As a result, substantial amounts of uncrystallized PP and POE underwent etching, resulting in the phenomenon of "large surface collapse", as depicted in Figure 5d. However, as the temperature decreased, PP crystal nuclei, some even in nano/microsized grains, gradually form during the saturation process before the final pressure removal step. Particularly, at the temperature of 120 °C, a large number of nano/microsized PP grains may be generated during the saturation process. After subsequent slow pressure release and rapid cooling, a well-defined grid-like PP crystallization network was successfully formed. Therefore, the etching part was mainly the POE phase. The relevant crystallization mechanism is illustrated in Figure 5e,f, where the orange part represents the continuous-phase PP region, the black solid part signifies the POE-enriched phase, and the red wavy line part indicates the PP crystallization region.

**3.4. Millimeter-Sized Cell Hole Phenomenon and Cell Opening Mechanism for the PP7/POE3 Blend.** As mentioned earlier, the PP7/POE3 foam prepared at 123 °C exhibited unexpectedly large cell holes, some even reaching millimeter-sized diameters (as shown in Figure S1). This led to a lack of oil−water selectivity. To investigate the underlying mechanism, we conducted a temperature−pressure orthogonal experiment, varying the pressure from 10 to 20 MPa and the temperature from 120 to 125 °C. The corresponding SEM micrographs are presented in Figure 6.

As depicted in the red dashed area, the phenomenon of large cell holes is not limited to 123 °C but is observed also in the high-pressure region at 120 °C and the low-pressure range at 125 °C. We attributed this phenomenon to a strong correlation with the $T_{c,onset}$ of PP in the PP7/POE3 matrix, which is 123


https://doi.org/10.1021/acsomega.3c07915
ACS Omega 2023, 8, 49372−49382

°C. For the case of the temperature at 123 °C, nano/microsized PP grains can be generated during the saturation process. During the last step of pressure relief, the ER value of the PP7/POE3 foam can reach 25−30 within the pressure range due to the appropriate melt strength. This high ER value is a result of the substantial biaxial stretching of the melt during cell growth. However, these grains in the melt are rigid materials that do not deform when stretched. With onset, the crystallization temperature could be changed owing to the plasticization of $CO_2$. Moreover, large holes could be attributed to the cell coalescence of the POE due to its poor melt strength under foaming conditions. As a result, fractures at the junction between the grains and the melt continue to propagate as the cells grow, ultimately leading to the formation of large cell holes.

However, when foamed at 120 °C, different from 123 °C, a greater quantity of crystal grains as well as larger grains may form during the saturation process. Attributed to the lower temperature and more crystal grains, the melt strength is higher than that at 123 °C. Because of the increased melt strength, the ER decreases to around 20. Consequently, the foam can expand and form open-cell structures without undergoing extensive ruptures. On the other hand, when foamed at 125 °C, which is higher than the $T_{c,onset}$ of PP, only a minimal number of crystal grains form during the saturation process. Although the melt strength at 125 °C is smaller than that at 123 °C, it exhibits better homogeneity due to fewer grains. As a result, in the pressure relief step, there is no significant occurrence of large-scale cell ruptures.

Interestingly, large cell holes occurred both at 123 °C and in the high-pressure region at 120 °C as well as the low-pressure region at 125 °C. We can conclude that when foaming within nearby temperature and pressure ranges, the foaming effect sometimes behaves equivalently, where an increase in temperature is similar to an increase in pressure and vice versa. This effect is primarily attributed to the plasticizing action of $CO_2$. As shown in Figure 6, the SEM micrographs at 120 °C and 20 MPa closely resemble those at 123 °C and 15 MPa, while the images at 125 °C and 10 MPa bear a striking resemblance to those at 123 °C and 17 MPa. This similarity arises from the equivalent influence of pressure and temperature on the melt strength of the polymer melt. Changes in pressure affect the solubility of $CO_2$ in the polymer melt, thereby impacting the melt strength, and the same holds true for temperature. Therefore, the appearance of the red dashed frames in the figures is a result of these factors.

The preparation methods of open-cell foams can be divided into a homogenous structure method and a heterogenous structure method. The heterogenous structure is realized by constructing the soft phase and hard phase.[45] In the two-step foaming process, the LCBPP/POE blend is initially melted at high temperatures and then cooled to the foaming temperature, typically within the range of 120−137 °C. During the foaming process triggered by the final stage of pressure relief, the cell walls exhibit structural inhomogeneity due to the coexistence of PP crystal grains, PP amorphous regions, and POE-enriched regions. Specifically, the PP crystal region serves as the hard phase, while the PP amorphous region and the POE-enriched region act as the soft phase. It is at the interface between these soft and hard phases where fractures can easily initiate. As cell growth continues, similar to biaxial stretching, the rigid nature of the crystal grains in the melt prevents deformation during stretching. Consequently, fractures at the interface between the soft and hard phases continue to propagate as the cells grow, ultimately resulting in the formation of an open-cell structure.

**3.5. Oil−Water Selective Properties of the LCBPP/POE Foam.** The ideal oil-absorbing material should possess the following characteristics: high oil/water selectivity, high oil−water separation capacity, high OCC, high oil absorption capacity, and excellent reusability. Therefore, different experimental characterizations were conducted to verify these characteristics.

To begin, a rectangular LCBPP/POE blend of the open-cell foam was prepared. The foam had dimensions of approximately 3 mm width, 6 mm length, and 2 mm height. Its hydrophobicity was evaluated through a water contact angle test (Figure 7a,b). The results demonstrated that the water

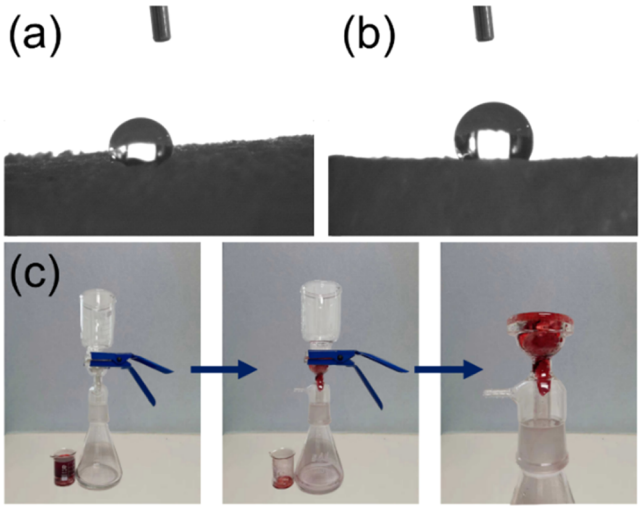


**Figure 7.** Water contact angle measurements for (a) PP and (b) PP7/POE3 foams. (c) Schematic diagram of oil−water selection performance.

contact angle of the pure PP foam was 97°, whereas that of the PP7/POE3 foam exceeded 140°, indicating the excellent hydrophobic nature of the PP7/POE3 foam.

Subsequently, the oil/water selectivity of the PP7/POE3 foam was assessed by using the solvent mixture comprising cyclohexane and water. The PP7/POE3 foam prepared at 130 °C and 13 MPa was selected for the oil−water selectivity experiment. Under the foaming conditions, the expansion ratio reaches 48 and the open cell content can reach 97.6%. As illustrated in Figure 7c, the open-cell PP7/POE3 foam was employed as a filter for oil/water separation. Following the filtration process, the liquid entering the Erlenmeyer flask underwent a visible transition from red to colorless. This transformation occurred due to the absorption of Sudan IV-labeled cyclohexane by the PP7/POE3 foam, while water flowed into the Erlenmeyer flask through the open-cell structure within the foam. These results substantiated the excellent oil absorption performance of the PP7/POE3 foam in water and its outstanding oil−water selectivity during the adsorption process.

**3.6. Oil Absorption Performance of the LCBPP/POE Foam.** The investigation reveals a noteworthy trend: despite the ER of PP/POE foams remaining relatively consistent across various POE content levels, there is a gradual increase in the oil absorption capacity as the POE content increases.


https://doi.org/10.1021/acsomega.3c07915
ACS Omega 2023, 8, 49372−49382

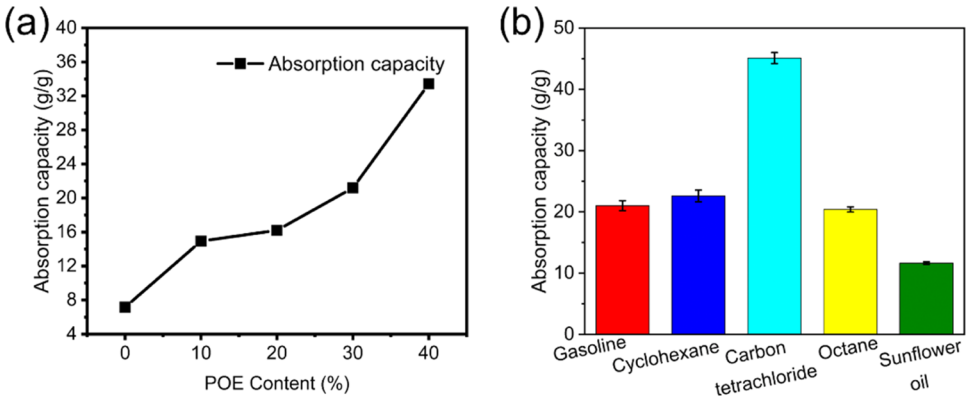


**Figure 8.** (a) Absorption capacity of the PP/POE-blended foam with different POE contents at 130 °C and 10 MPa. (b) Adsorption capacity of different oils of the PP7/POE3 foam.

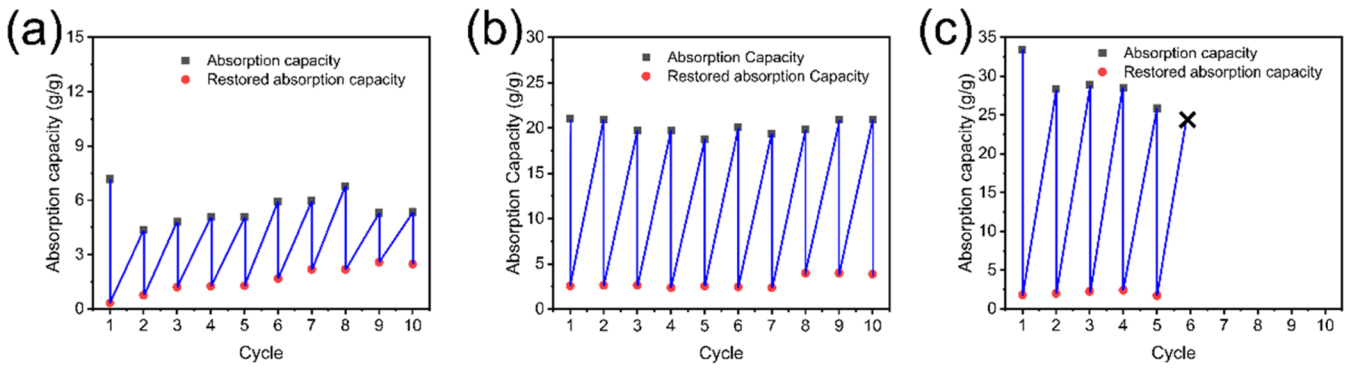


**Figure 9.** Repeated oil absorption diagrams of (a) pure PP, (b) PP7/POE3, and (c) PP6/POE4 foams at 130 °C and 13 MPa.

Figure 8a provides a visual representation of the oil absorption capacity of the LCBPP/POE foam at different POE ratios. This chart illustrates that foams containing higher levels of POE exhibit superior oil absorption capabilities. The data highlight the oil absorption capacity of the LCBPP/POE foam at varying ratios of PP to PP6/POE4, registering at 7.17, 14.94, 16.20, 21.03, and 33.43 g/g. The rationale behind this phenomenon lies in the fact that foams with greater POE contents boast higher OCCs, leading to enhanced oil absorption capacity. Specifically, the PP7/POE3 foam achieves an impressive maximum OCC of 97.6%, whereas pure PP lags behind at 83.3%.

While the PP6/POE4 foam exhibits the highest OCC of 98.3%, the excessive addition of POE renders the resulting foams too fragmented to withstand cyclic oil absorption experiments. In this context, we turned to the PP3/POE7 foam to assess absorption capacities across various oil types. As depicted in Figure 8b, the PP3/POE7 foam demonstrates absorption capacities of 21.0, 22.8, 45.1, 20.4, and 10.625 g/g for gasoline, cyclohexane, carbon tetrachloride, octane, and sunflower oil, respectively. Compared with other studies, the open-cell PP foam prepared in this study has a relatively high oil absorption capacity.

**3.7. Reusability of the LCBPP/POE Foam.** Reusability stands out as a crucial attribute in oil absorption foams. A foam's capacity to bounce back after compression deformation greatly enhances its potential for recovery and subsequent reuse in oil absorption cycles. In this investigation, the reusability of LCBPP/POE foams was assessed through cyclic oil absorption tests.

During the initial adsorption, the open-cell foam reached saturation with the absorbed gasoline. Subsequent compression led to the expulsion of most of the gasoline. In the subsequent cyclic adsorption−desorption experiment, the foam once again absorbed gasoline to saturation and regained its original dimensions.

Figure 9 shows the weight-based oil absorption of the LCBPP/POE foam with varying POE content for gasoline. The results indicated that the oil absorption capacity for gasoline in PP and PP7/POE3 was 7.17 and 21.01 g/g, respectively. After 10 cycles of adsorption and desorption, their oil absorption capacities remained at 5.36 and 20.86 g/g, respectively. This signifies that the PP7/POE3 foam exhibits a superior oil absorption capacity compared to that of the pure PP foam. Remarkably, the oil absorption capacity of the PP7/POE3 foam after 10 cycles reaches 99.3% of its initial capacity, a proof of its excellent resistance to shrinkage. (Cyclic oil absorption test results for PP7/POE3 foams prepared under different temperature and pressure conditions are detailed in Figure S5.)

Although PP6/POE4 attains a maximum oil absorption capacity of 33.43 g/g, its cell walls deteriorate after only four cycles and the cell structure cannot be adequately maintained. Consequently, further cyclic oil absorption experiments for the PP6/POE4 foam were discontinued.

If the foam exhibits good recoverability after compression deformation, it will be beneficial for the foam to be recovered and reused for oil absorption in the next cycle. Cyclic compression was conducted on open-cell foam plastics from PP to PP7/POE3 to study their recoverability after compression deformation (Figure 10). The foam was com-


https://doi.org/10.1021/acsomega.3c07915
ACS Omega 2023, 8, 49372−49382

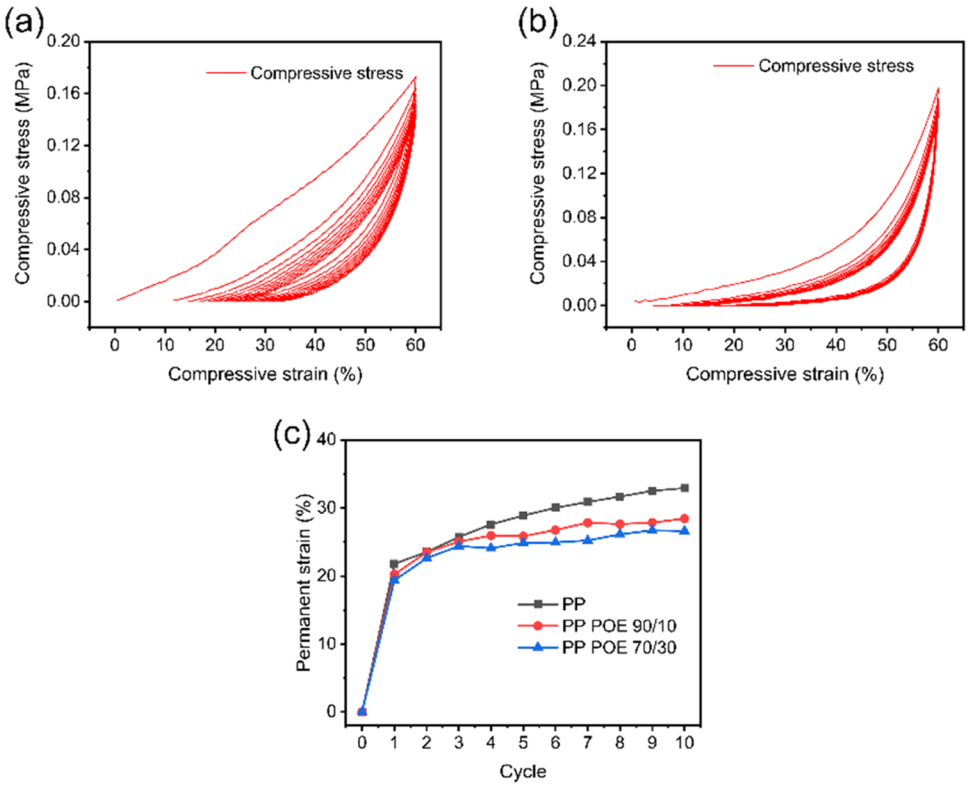


**Figure 10.** 10-cycle compression behavior of the PP/POE open-cell foam: (a) PP and (b) PP7/POE3. (c) Permanent strain of the PP/POE-coblended foam with cycles.

pressed for 10 cycles with a maximum strain of 60%. The cyclic compression stress−strain curve showed that the maximum stress of PP and PP7/POE3 foam plastics was about 170 and 190 kPa, respectively. This indicates that the rigidity of the PP7/POE3 foam plastic is lower than that of the pure PP foam plastic, which is attributed to the elastic component in the blend. After the first compression, the permanent strain of PP and PP7/POE3 foam plastics was about 24 and 17%, respectively. They were easier to recover after compression. With the increase of compression cycles of PP and PP7/POE3 foam plastics, the permanent strain of both foam plastics increased and the permanent strain of the latter increased less.

Figure 10 summarizes the permanent strain of PP/POE foams with different POE contents after different cycles. The results showed that the permanent strain increased with increasing cycle times and decreased with increasing POE content.

## 4. CONCLUSIONS

In summary, this study successfully prepared open-cell LCBPP/POE foams and explored their oil absorption performance. Through the implementation of a two-step foaming method, we achieved LCBPP/POE foams with high expansion ratios and open cell contents. The optimal LCBPP/POE ratio for desirable foaming properties was identified as 70/30%. This ratio allowed for precise control of the cell diameter and facilitated the creation of a mechanically stable open-cell structure. The ideal foaming temperature and pressure conditions were determined based on expansion ratio and open cell content measurements.

The resulting PP7/POE3 foam exhibited remarkable characteristics, including an impressive open cell content of 97.6%, enhanced oil absorption efficiency of 21.01 g/g, and outstanding reusability, maintaining 99.3% of its original oil absorption capacity after 10 cycles of adsorption and desorption. These improvements can be attributed to the incorporation of the POE, which enhanced the foam's hydrophobic and oleophilic properties as well as its ability to repeatedly absorb oil.

In conclusion, the open-cell LCBPP/POE blend foam holds great promise as an efficient oil absorbent, offering potential applications in addressing oil spill cleanup and related challenges.

## ■ ASSOCIATED CONTENT

### Supporting Information

The Supporting Information is available free of charge at https://pubs.acs.org/doi/10.1021/acsomega.3c07915.

Cross-section of the PP7/POE3 foam sample at 123 °C, SEM micrographs of pure PP at different temperatures after quenching under carbon dioxide and etching with xylene, SEM micrographs of PP7/POE3 foam samples at 15 MPa, SEM micrographs of the pure PP foam at 120, 130, and 137 °C, SEM micrograph of the pure POE foam at 130 °C, and repeated oil absorption diagrams of the PP7/POE3 open-cell foam at 127 °C, 133 °C, and 130 °C and 13 MPa (PDF)

## ■ AUTHOR INFORMATION

### Corresponding Authors

**Li Zhang** − *School of Materials Science and Chemical Engineering, Ningbo University, Ningbo 315211, China; Key Laboratory of Impact and Safety Engineering, Ministry of Education, Ningbo University, Ningbo 315211, China;*



https://doi.org/10.1021/acsomega.3c07915
*ACS Omega* 2023, 8, 49372−49382

orcid.org/0000-0003-2684-0414; Email: zhangli2@nbu.edu.cn

**Jinbiao Bao** − *Ningbo Micro-Foam Technology Co., Ltd., High-Tech Zone, Ningbo 315048, China*; Email: baojinbiao@micro-foam.com

### Authors

**Chenhui Li** − *School of Materials Science and Chemical Engineering, Ningbo University, Ningbo 315211, China; Key Laboratory of Impact and Safety Engineering, Ministry of Education, Ningbo University, Ningbo 315211, China*

**Jirun Hu** − *Goettfert (China) Limited, Shanghai 200083, China*

**Haikuo Yan** − *National Engineering Lab of Textile Fiber Materials & Processing Technology (Zhejiang), Zhejiang Sci-Tech University, Hangzhou 310018, China*

**Yuyuan Yao** − *National Engineering Lab of Textile Fiber Materials & Processing Technology (Zhejiang), Zhejiang Sci-Tech University, Hangzhou 310018, China*; orcid.org/0000-0002-4239-6061

Complete contact information is available at: https://pubs.acs.org/10.1021/acsomega.3c07915

### Notes

The authors declare no competing financial interest.

## ■ ACKNOWLEDGMENTS

This work was financially supported by the Municipal Key R&D Program of Ningbo (No. 2023Z088) and the K. C. Wong Magna Fund in Ningbo University.

## ■ REFERENCES

(1) Zhang, A. J.; Chen, M. J.; Du, C.; Guo, H. Z.; Bai, H.; Li, L. Poly(dimethylsiloxane) Oil Absorbent with a Three-Dimensionally Interconnected Porous Structure and Swellable Skeleton. *ACS Appl. Mater. Interfaces* **2013**, *5* (20), 10201−10206.

(2) Lee, J. H.; Kim, D. H.; Kim, Y. D. High-performance, recyclable and superhydrophobic oil absorbents consisting of cotton with a polydimethylsiloxane shell. *J. Ind. Eng. Chem.* **2016**, *35*, 140−145.

(3) Yang, C.; Zhang, Q.; Zhang, W.; Xia, M.; Yan, K.; Lu, J.; Wu, G. High thermal insulation and compressive strength polypropylene microcellular foams with honeycomb structure. *Polym. Degrad. Stab.* **2021**, *183*, No. 109406.

(4) Huang, Y. F.; Gancheva, T.; Favis, B. D.; Abidli, A.; Wang, J.; Park, C. B. Hydrophobic Porous Polypropylene with Hierarchical Structures for Ultrafast and Highly Selective Oil/Water Separation. *ACS Appl. Mater. Interfaces* **2021**, *13* (14), 16859−16868.

(5) Shi, Y. L.; Feng, X. J.; Yang, R. H. Preparation of recyclable corn straw fiber as oil absorbent via a one-step direct modification. *Mater. Res. Express* **2021**, *8* (1), No. 015506.

(6) Lee, J. H.; Kim, D. H.; Han, S. W.; Kim, B. R.; Park, E. J.; Jeong, M. G.; Kim, J. H.; Kim, Y. D. Fabrication of superhydrophobic fibre and its application to selective oil spill removal. *Chem. Eng. J.* **2016**, *289*, 1−6.

(7) Shi, G. Y.; Qian, Y. Z.; Tian, F. Z.; Cai, W. J.; Li, Y.; Cao, Y. F. Controllable synthesis of pomelo peel-based aerogel and its application in adsorption of oil/organic pollutants. *R. Soc. Open Sci.* **2019**, *6* (2), No. 181823.

(8) Ghasemi, O.; Mehrdadi, N.; Baghdadi, M.; Aminzadeh, B.; Ghaseminejad, A. Spilled oil absorption from Caspian sea water by graphene/chitosan nano composite. *Energy Sources, Part A* **2020**, *42* (23), 2856−2872.

(9) Zhou, X. Y.; Zhang, Z. Z.; Xu, X. H.; Men, X. H.; Zhu, X. T. Facile Fabrication of Superhydrophobic Sponge with Selective Absorption and Collection of Oil from Water. *Ind. Eng. Chem. Res.* **2013**, *52* (27), 9411−9416.

(10) Wu, L.; Li, L. X.; Li, B. C.; Zhang, J. P.; Wang, A. Q. Magnetic, Durable, and Superhydrophobic Polyurethane@Fe3O4@SiO2@Fluoropolymer Sponges for Selective Oil Absorption and Oil/Water Separation. *ACS Appl. Mater. Interfaces* **2015**, *7* (8), 4936−4946.

(11) Wang, H. Y.; Wang, E. Q.; Liu, Z. J.; Gao, D.; Yuan, R. X.; Sun, L. Y.; Zhu, Y. J. A novel carbon nanotubes reinforced superhydrophobic and superoleophilic polyurethane sponge for selective oil-water separation through a chemical fabrication. *J. Mater. Chem. A* **2015**, *3* (1), 266−273.

(12) Wang, S. S.; Yang, W. J.; Li, X. P.; Hu, Z. L.; Wang, B.; Li, M. J.; Dong, W. P. Preparation of high-expansion open-cell polylactic acid foam with superior oil-water separation performance. *Int. J. Biol. Macromol.* **2021**, *193*, 1059−1067.

(13) Xiao, W. L.; Niu, B. H.; Yu, M.; Sun, C. D.; Wang, L. H.; Zhou, L.; Zheng, Y. Fabrication of foam-like oil sorbent from polylactic acid and Calotropis gigantea fiber for effective oil absorption. *J. Cleaner Prod.* **2021**, *278*, No. 123507.

(14) Lopez-Gonzalez, E.; Saiz-Arroyo, C.; Rodriguez-Perez, M. A. Low-density open-cell flexible polyolefin foams as efficient materials for oil absorption: influence of tortuosity on oil absorption. *Int. J. Environ. Sci. Technol.* **2020**, *17* (3), 1663−1674.

(15) Rizvi, A.; Chu, R. K. M.; Lee, J. H.; Park, C. B. Superhydrophobic and Oleophilic Open-Cell Foams from Fibrillar Blends of Polypropylene and Polytetrafluoroethylene. *ACS Appl. Mater. Interfaces* **2014**, *6* (23), 21131−21140.

(16) Nam, C.; Li, H. X.; Zhang, G.; Chung, T. C. M. Petrogel: New Hydrocarbon (Oil) Absorbent Based on Polyolefin Polymers. *Macromolecules* **2016**, *49* (15), 5427−5437.

(17) Ren, Q.; Dai, T.; Jin, X. Y.; Wu, D.; Wang, C. Y.; Li, J.; Zhu, S. P. Solution Processed Coating of Polyolefin on Melamine Foams to Fabricate Tough Oil Superabsorbents. *Macromol. Mater. Eng.* **2018**, *303* (12), No. 1800436.

(18) Huang, P. K.; Wu, F.; Shen, B.; Ma, X. H.; Zhao, Y. Q.; Wu, M. H.; Wang, J.; Liu, Z. H.; Luo, H. B.; Zheng, W. G. Bio-inspired lightweight polypropylene foams with tunable hierarchical tubular porous structure and its application for oil-water separation. *Chem. Eng. J.* **2019**, *370*, 1322−1330.

(19) Huang, P.; Su, Y.; Wu, F.; Lee, P. C.; Luo, H.; Lan, X.; Zhang, L.; Shen, B.; Wang, L.; Zheng, W. Extruded polypropylene foams with radially gradient porous structures and selective filtration property via supercritical CO2 foaming. *J. $CO_2$ Util.* **2022**, *60*, No. 101995.

(20) Mi, H.-Y.; Jing, X.; Liu, Y.; Li, L.; Li, H.; Peng, X. F.; Zhou, H. Highly Durable Superhydrophobic Polymer Foams Fabricated by Extrusion and Supercritical CO2 Foaming for Selective Oil Absorption. *ACS Appl. Mater. Interfaces* **2019**, *11* (7), 7479−7487.

(21) Sun, Y.; Ma, L. Y.; Song, Y. F.; Phule, A. D.; Li, L.; Zhang, Z. X. Efficient natural rubber latex foam coated by rGO modified high density polyethylene for oil-water separation and electromagnetic shielding performance. *Eur. Polym. J.* **2021**, *147*, No. 110288.

(22) Kmetty, A.; Tomin, M.; Barany, T.; Czigany, T. Static and dynamic mechanical characterization of cross-linked polyethylene foams: The effect of density. *Express Polym. Lett.* **2020**, *14* (5), 503−509.

(23) Wu, T.; Xu, W. H.; Guo, K.; Xie, H.; Qu, J. P. Efficient fabrication of lightweight polyethylene foam with robust and durable superhydrophobicity for self-cleaning and anti-icing applications. *Chem. Eng. J.* **2021**, *407*, No. 127100.

(24) Kong, W. L.; Bao, J. B.; Wang, J.; Hu, G. H.; Xu, Y.; Zhao, L. Preparation of open-cell polymer foams by CO2 assisted foaming of polymer blends. *Polymer* **2016**, *90*, 331−341.

(25) Fang, Y. W.; Bao, J. B.; Yan, H. K.; Sun, W.; Zhao, L.; Hu, G. H. Preparation of open-cell foams from polymer blends by supercritical $CO_2$ and their efficient oil-absorbing performance. *AIChE J.* **2016**, *62* (12), 4182−4185.

(26) Zhao, J. C.; Huang, Y. F.; Wang, G. L.; Qiao, Y. N.; Chen, Z. L.; Zhang, A. M.; Park, C. B. Fabrication of outstanding thermal-insulating, mechanical robust and superhydrophobic PP/CNT/sorbitol derivative nanocomposite foams for efficient oil/water separation. *J. Hazard. Mater.* **2021**, *418*, No. 126295.

(27) Wang, S. S.; Wang, K.; Pang, Y. Y.; Li, Y.; Wu, F.; Wang, S.; Zheng, W. G. Open-cell polypropylene/polyolefin elastomer blend foams fabricated for reusable oil-sorption materials. *J. Appl. Polym. Sci.* **2016**, *133* (33), No. 43812, DOI: 10.1002/app.43812.
(28) Pang, Y. Y.; Wang, S. S.; Wu, M. H.; Liu, W.; Wu, F.; Lee, P. C.; Zheng, W. G. Kinetics study of oil sorption with open-cell polypropylene/polyolefin elastomer blend foams prepared via continuous extrusion foaming. *Polym. Adv. Technol.* **2018**, *29* (4), 1313−1321.
(29) Naguib, H. E.; Park, C. B.; et al. Strategies for achieving ultra low-density polypropylene foams. *Polym. Eng. Sci.* **2002**, *42* (7), 1481−1492.
(30) Xu, Z. M.; Jiang, X. L.; Liu, T.; Hu, G. H.; Zhao, L.; Zhu, Z. N.; Yuan, W. K. Foaming of polypropylene with supercritical carbon dioxide. *J. Supercrit. Fluids* **2007**, *41* (2), 299−310.
(31) Ameli, A.; Jung, P. U.; Park, C. B. Electrical properties and electromagnetic interference shielding effectiveness of polypropylene/carbon fiber composite foams. *Carbon* **2013**, *60*, 379−391.
(32) Ameli, A.; Nofar, M.; Park, C. B.; Potschke, P.; Rizvi, G. Polypropylene/carbon nanotube nano/microcellular structures with high dielectric permittivity, low dielectric loss, and low percolation threshold. *Carbon* **2014**, *71*, 206−217.
(33) Yetgin, S. H.; Unal, H.; Mimaroglu, A. Influence of foam agent content and talc filler on the microcellular and mechanical properties of injection molded polypropylene and talc filled polypropylene composite foams. *J. Cell. Plast.* **2014**, *50* (6), 563−576.
(34) Yang, C. G.; Wang, M. H.; Zhang, M. X.; Li, X. H.; Wang, H. L.; Xing, Z.; Ye, L. F.; Wu, G. Z. Supercritical CO2 Foaming of Radiation Cross-Linked Isotactic Polypropylene in the Presence of TAIC. *Molecules* **2016**, *21* (12), 1660.
(35) Stange, J.; Uhl, C.; Münstedt, H. Rheological behavior of blends from a linear and a long-chain branched polypropylene. *J. Rheol.* **2005**, *49* (5), 1059−1079.
(36) Zulli, F.; Andreozzi, L.; Passaglia, E.; Augier, S.; Giordano, M. Rheology of long-chain branched polypropylene copolymers. *J. Appl. Polym. Sci.* **2013**, *127* (2), 1423−1432.
(37) Huang, J.; He, G.; Liao, X.; Huang, Y.; Yang, Q. The rheological property and foam morphology of linear polypropylene and long chain branching polypropylene. *J. Wuhan Univ. Technol.-Mater. Sci. Ed.* **2013**, *28* (4), 798−803.
(38) Wang, K.; Wang, S.; Wu, F.; Pang, Y.; Liu, W.; Zhai, W.; Zheng, W. A new strategy for preparation of long-chain branched polypropylene via reactive extrusion with supercritical $CO_2$ designed for an improved foaming approach. *J. Mater. Sci.* **2016**, *51*, 2705−2715.
(39) Wang, L.; Ishihara, S.; Ando, M.; Minato, A.; Hikima, Y.; Ohshima, M. Fabrication of high expansion microcellular injection-molded polypropylene foams by adding long-chain branches. *Ind. Eng. Chem. Res.* **2016**, *55* (46), 11970−11982.
(40) Du, B.; Chen, S. T.; Zhang, F. B.; Shi, X. B.; Li, R. B. Nonlinear Rheological Behavior of Long Chain Branching Polypropylene. *Chem. J. Chin. Univ.-Chin.* **2021**, *42* (6), 2034−2040.
(41) Hou, J. J.; Zhao, G. Q.; Zhang, L.; Wang, G. L.; Li, B. High-expansion polypropylene foam prepared in non-crystalline state and oil adsorption performance of open-cell foam. *J. Colloid Interface Sci.* **2019**, *542*, 233−242.
(42) Yang, H.; Zhang, X. Q.; Qu, C.; Li, B.; Zhang, L. J.; Zhang, Q.; Fu, Q. Largely improved toughness of PP/EPDM blends by adding nano-SiO2 particles. *Polymer* **2007**, *48* (3), 860−869.
(43) Cao, J.; Zhao, Z. Y.; Du, R. N.; Zhang, Q.; Fu, Q. Effect of beta nucleating agent on mechanical properties of PP/POE blends. *Plast., Rubber Compos.* **2007**, *36* (7−8), 320−325.
(44) Zhang, Y. J.; Jiang, X. Y.; Bai, Z. W.; Wang, J. K.; Qian, Z. M.; Liu, Y. X. Re-treated nanocellulose whiskers alongside a polyolefin elastomer to toughen and improve polypropylene composites. *J. Appl. Polym. Sci.* **2018**, *135* (15), 46066.
(45) Li, C.; Ye, H.; Ge, S.; Yao, Y.; Ashok, B.; Hariram, N.; Rajulu, A. V.; et al. Fabrication and properties of antimicrobial flexible nanocomposite polyurethane foams with in situ generated copper nanoparticles. *J. Mater. Res. Technol.* **2022**, *19*, 3603−3615.


https://doi.org/10.1021/acsomega.3c07915
*ACS Omega* 2023, 8, 49372−49382